Геология и геофизика, *т. 65, № 9, с. 1302—1316,* DOI: 10.15372/GiG2024103, EDN: MOHOWI
Поступила в редакцию 06.06.2023, принята в печать 10.01.2024 *Опубликована онлайн: 13.01.2024*

УДК

ДЕТЕРМИНИСТИЧЕСКОЕ И СТОХАСТИЧЕСКОЕ МОДЕЛИРОВАНИЕ В ПРОГНОЗИРОВАНИИ ПЕТРОФИЗИЧЕСКИХ СВОЙСТВ АЛЬБСКОГО КАРБОНАТНОГО КОЛЛЕКТОРА В БАССЕЙНЕ КАМПОС (*Юго-Восточная Бразилия*)

А. Карраскилья, Р. Гуэрра

Laboratory of Engineering and Exploration of Petroleum (LENEP), Darcy Ribeiro Northern Rio de Janeiro State University, Amaral Peixoto Highway, Km 163, Brennand Avenue, S/N, Imboacica, Macaé, RJ, 27925310, Brazil

Проницаемость является одним из наиболее важных и сложных параметров для оценки при характеристике нефтяного коллектора. Косвенная оценка проницаемости осуществлялась несколькими эмпирическими методами с использованием скважинных геофизических данных. Они включают в себя модель Тимура, в которой используются обычные каротажи, и модель Тимура — Коутса, в которой используется каротаж ядерного магнитного резонанса. Первой целью исследования была оценка пористости, поскольку она напрямую влияет на оценки проницаемости. Затем были проведены детерминистическая и стохастическая инверсии, потому что основной целью работы была оценка проницаемости карбонатного коллектора в бассейне Кампос на юго-востоке Бразилии. Схема гребневой регрессии была использована для детерминистической инверсии уравнений Тимура и Тимура — Коутса. Стохастическая инверсия позже была решена с использованием нечеткой логики в качестве прямой задачи, а для оценки неопределенности был применен метод Монте-Карло. Все оценки были проверены на соответствие лабораторным данным по пористости и проницаемости с использованием коэффициента корреляции Пирсона (R), среднеквадратичной ошибки (RMSE), средней абсолютной ошибки (MAE) и индекса согласия Уиллмотта (d). Результаты для модели Тимура составили $R = 0.41$; RMSE = 333.28; MAE = 95.56; и $d = 0.55$. Эти значения были хуже для модели Тимура — Коутса: $R = 0.39$; RMSE = 355.28; MAE = 79.35; и $d = 0.51$. Модель Тимура с зонами течения продемонстрировала результаты $R = 0.55$; RMSE = 210.88; MAE = 116.66; и $d = 0.84$, что превосходило результаты для двух других моделей. Таким образом, детерминистическая инверсия показала слабую способность адаптироваться к значительным колебаниям значений проницаемости вдоль скважины, что видно из сравнения этих трех подходов. Однако стохастическая инверсия с использованием трех ячеек дала результаты $R = 0.35$; RMSE = 320.27; MAE = 190.93; и $d = 0.73$, что выглядело хуже, чем результаты детерминистической инверсии. Тем временем стохастическая инверсия с шестью ячейками успешно скорректировала набор лабораторных наблюдений, поскольку она обеспечивает $R = 0.87$; RMSE = 156.81; MAE = 74.60; и $d = 0.92$. Доказано, что последний подход может обеспечить надежное решение с согласованными параметрами и точной оценкой проницаемости.

Карбонатный коллектор, инверсия, пористость, проницаемость, гребневая регрессия, схема нечеткой логики, анализ неопределенности методом Монте-Карло

DETERMINISTIC AND STOCHASTIC MODELING IN PREDICTION OF PETROPHYSICAL PROPERTIES OF AN ALBIAN CARBONATE RESERVOIR IN THE CAMPOS BASIN (*Southeastern Brazil*)

A. Carrasquilla, R. Guerra

Permeability is one of the most significant and challenging parameters to estimate when characterizing an oil reservoir. Several empirical methods with geophysical borehole logs have been employed to estimate it indirectly. They include the Timur model, which uses conventional logs, and the Timur–Coates model, which uses the nuclear magnetic resonance log. The first goal of this study was to evaluate porosity, because it directly impacts permeability estimates. Deterministic and stochastic inversions were then carried out, as the main objective of this work was to estimate the permeability in a carbonate reservoir of the Campos Basin, Southeastern Brazil. The ridge regression scheme was used to invert the Timur and Timur–Coates equations deterministically. The stochastic inversion was later solved using fuzzy logic as the forward problem, and the Monte Carlo method was utilized to assess uncertainty. The goodness of fit for the estimations was all checked with porosity and permeability laboratory data using the Pearson correlation coefficient (R), root mean square error (RMSE), mean absolute error (MAE), and Willmott's agreement index (d). The results for the Timur model were $R = 0.41$; RMSE = 333.28; MAE = 95.56; and $d = 0.55$. These values were worse for the Timur–Coates model, with $R = 0.39$; RMSE = 355.28; MAE = 79.35; and $d = 0.51$. The Timur model with flow zones had $R = 0.55$; RMSE = 210.88; MAE = 116.66; and $d = 0.84$, which outperformed the other two models. The deterministic inversion showed, thus, little ability to adapt to the significant variations of the permeability values along the

✉e-mail: abel@lenep.uenf.br

well, as can be seen from comparing these three approaches. However, the stochastic inversion using three bins had $R = 0.35$; RMSE = 320.27; MAE = 190.93; and $d = 0.73$, looking worse than the deterministic inversion. In the meantime, the stochastic inversion with six bins successfully adjusted the set of laboratory observations, because it provides $R = 0.87$; RMSE = 156.81; MAE = 74.60; and $d = 0.92$. This way, the last approach has proven it can produce a reliable solution with consistent parameters and an accurate permeability estimation.

Keywords: carbonate reservoir, inversion, porosity, permeability, ridge regression, fuzzy logic scheme, Monte Carlo uncertainty analysis

INTRODUCTION

In the oil industry, petrophysical characteristics, such as lithology, porosity, permeability, and water saturation, affect the well productivity in hydrocarbon-bearing reservoirs. Geophysical well logs, one of the most valuable and essential tools for rock evaluation, are one way of assessing these reservoir properties. Nowadays, logs serve as a continuous and complete record for appraising the geologic formations that a borehole crosses (Luthi, 2001). The signals captured by the tools in the subsurface media are translated into the attributes to assess reservoir rock formation and identify fluid types. This procedure enables us to operate the wellbore, to correlate formation depths with nearby wells, and to make interpretations of the quantity and quality of the petroleum present. Nevertheless, they do not directly present these relevant properties to calculate the financial potential of the geologic formations (Tiab and Donaldson, 2015).

Reservoir rock has to be porous and permit fluid flow through the interconnected spaces to be commercially viable. One of the critical parameters to be estimated in the characterization of an oil reservoir is permeability, which is the capacity of conducting fluids (Doveton, 2014). It is a critical variable for comprehending fluid movement behavior, and in the oil and gas sector, predicting it accurately is an important problem and a key component of reservoir characterization. The accurate permeability estimation aids in reservoir development and production strategy optimization. Owing to the influence of various geologic factors that regulate fluid circulation, this prediction is a challenge (Lucia, 2007).

The typical method for determining permeability is to conduct time- and money-consuming laboratory experiments directly on core or sidewall samples, well testing, and analog reservoir investigations (Liu, 2017). These methods only examine a small portion of the reservoir, so one should search for methods that can be used throughout the reservoir. In addition to these direct methods, this estimate can be made using indirect methods like logs (Schön, 2015). Empirical models developed by Tixier (1949), Morris and Biggs (1967), Timur (1968), Coates and Dumanoir (1974), Coates and Denoo (1981), Coates et al. (1999), and Lacentre and Carrica (2003) have been used in numerous attempts to determine the permeability from logs over time. Therefore, log-based permeability predictions may have drawbacks because of presumptions and uncertainties in the empirical relationships, though they are relatively quicker and less expensive. According to Kennedy (2015), most petrophysical parameters are typically correlated with well-log data. However, no evident and significant correlation exists between reservoir permeability and log data. Multiple linear regression (Wendt et al., 1986), multivariate analysis (Lee and Datta-Gupta, 1999), and polynomial regression (Ahangar-Asr et al., 2011), among others, used logs as input to perform this estimation. Additionally, theoretical–mathematical models by Kozeny and Carman (Bernabé et al., 2010), Katz and Thompson (1986), Schwartz, Sen, and Johnson (Johnson et al., 1986), and Glover and Walker (2009) have all been used to estimate permeability. Artificial intelligence techniques, such as fuzzy logic (Hambalek and Gonzalez, 2003; Ilkhchi et al., 2006), neural networks (Huang et al., 1996), support vector learning (Weston et al., 1999), and genetic algorithms (Wang et al., 2020), have also been used in recent years to predict the permeability of oil reservoirs.

Since 1940, mathematical and physical problems have been solved using Monte Carlo methods, which are most valuable when it is challenging to use other strategies. They comprise a large group of computational algorithms that rely on repeated random sampling to produce numbers. The underlying idea is to use randomness to find solutions to issues that, theoretically, could be deterministic. These techniques are typically used to generate sketches from a probability distribution, integrate numerically, and solve optimization problems. In many fields, including chemistry, physics, engineering, biology, medicine, etc., the technique has been used to estimate permeability (Cao et al., 2022). Numerous studies have been conducted in the petroleum field, including those by Tao and Watson (1984), Adams (2005), Kumar and Varghese (2005), Yu et al. (2005), Vadapalli et al. (2014), Fazelabdolabadi et al. (2019), Francioli and Carrasco (2019), Inyang et al. (2019), and Guerra (2020).

Using well-log data to determine petrophysical characteristics of oil reservoirs, such as permeability, is a common task for all the reasons that have been previously mentioned (Wyllie and Rose, 1950). Even so, predicting permeability from logs is complicated and far from an exact science. As a result, determining permeability is complex, and numerous additional attempts will be made in the future (Esmailzadeh et al., 2017). The

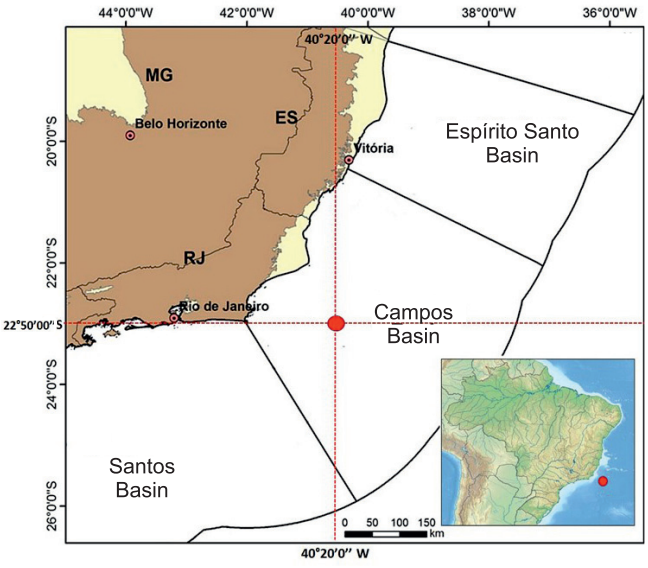

Fig. 1. Location map of the studied oilfield in the Campos Basin (modified from (Bruhn et al., 2003)).

permeability estimation is, therefore, the focus of this work. Inverse mathematical techniques, deterministic and stochastic, were used to interpret the results after using log data as the evaluation input. The logs were initially interpreted to identify where the hydrocarbons were present. Initially, the porosity was calculated for each geologic stratum, since the permeability estimate depends on this assessment. Then, with the application of Timur's (1968) equation, which used basic logs for the calculation of permeability, and the Timur–Coates (Coates et al., 1999) equation, which uses the Nuclear Magnetic Resonance (NMR) log, the deterministic inversion analysis was carried out. Based on these methods, an algorithm was created to estimate the reservoir permeability using the ridge regression technique (Alkinani et al., 2022). After that stochastic inversion was created using the fuzzy logic (FL) method as the forward problem, which takes the conventional logs as input. Monte Carlo (MC) error analysis, which offers quantifiable accuracy measures, was then used to analyze the estimated permeability quality (Cuddy and Glover, 2002).

Francioli and Carrasco (2019) used log data as input and laboratory measurements on rock samples to validate petrophysical parameters, such as porosity, clay volume, water saturation, and permeability. They estimated these properties using FL and analyzed the probability distributions utilizing the MC technique to quantify the assessment uncertainties. Both studies were conducted in carbonate reservoirs, but the datasets are different, our postsalt and their presalt layers. Additionally, the permeability was the only focus of the study, and inverse deterministic estimates of the log empirical equations by Timur and Timur and Coates were made using basic logs and the NMR log, respectively. With experimental permeability data from rock samples, the results were confirmed. The deterministic FL permeability estimate used basic logs as input and was verified with experimental data on rock samples. The stochastic MC technique was then used to evaluate the permeability estimation uncertainties.

GEOLOGIC CONTEXT

The reservoir addressed in this study belongs to the Campos Basin, which is in Southeastern Brazil (Fig. 1). The origin and evolution of the Campos Basin are related to the separation of the supercontinent Gondwana. They are marked by the disaggregation of the South American and African plates with the consequent formation of the South Atlantic Ocean (Bruhn et al., 2003). The tectonic and sedimentary evolution of this basin occurred in three primary megasequences: rift, postrift, and drift phases (Guardado et al., 1989), which correspond, respectively, to the continental, transitional, and marine systems and comprise a wide variety of reservoirs (Dias et al., 1990).

The marine sequence begins the open marine deposition during thermal subsidence associated with the drift phase. This stage begins with carbonate sedimentation (Macaé Group) and grades to a mainly siliciclastic succession (Campos Group), all affected by intense halokinesis (Supplementary Materials, Fig. 1). In an early drift context, the Macaé Group sedimentation occurred during the Albian Age and comprised the Goitacás, Quissamã, Outeiro, Imbetiba, and Namorado formations. The Quissamã Formation comprises grainstone and packstone carbonate rocks consisting of oncoids, ooids, peloids, and other bioclasts. It is associated with NE shoals deposited in high- to moderate-energy environments. The Outeiro Formation is formed of thin carbonate layers interbedded with marl and mudstone deposited in response to a gradual rise in sea level and the drowning of the shallow carbonate platform of the Quissamã Formation (Suppl. Mat., Fig. 2). These carbonate rocks have abundant pelagic microfossils like calcispheres (pithonellids), planktonic foraminifera, and radiolarians (Okubo et al., 2015).

MATERIALS AND METHODS

The works by Kozeny (1927), Carman (1937), Tixier (1949), Morris and Biggs (1967), Timur (1968), Coates and Denoo (1974), Coates and Dumanoir (1974), Amaefule et al. (1993), Timur and Coates (Coates et

al., 1999), and Lacentre and Carrica (2003) are just a few of the many initiatives in estimating permeability over time. The studies of Timur and Timur and Coates, the first using basic logs and the second using the NMR log as input, were concentrated on this work.

Kozeny (1927) first proposed the equation for determining the rock permeability, and Carman (1937) later modified it. The Kozeny–Carman equation, a classical permeability–porosity relationship, is used in various fields, including chemical, biochemical, and electrochemical engineering, groundwater flow, and water and oil reservoirs. Still, many other permeability models commonly use this equation as their foundation:

$$k = a\frac{\phi^3}{S^2\left(1-\phi\right)^2}, \tag{1}$$

where k = permeability (m^2); a = 0.2 is the Kozeny constant, which depends on pore shapes; S is the specific surface area of the rock (m^{-1}); and ϕ is the porosity (fraction). The formula only applies to groups of sphere-shaped rocks, and the surface area can only be calculated using core analysis and specialized tools. It is based on flow through capillary tubes, and a sample with cross-sectional area A and length L is made up of n capillary tubes, each with microscopic length l and radius r, representing rock with connected pores. The measure of rock texture that connects permeability with average grain diameter is called "the porosity function" ($\phi^3/(1-\phi)^2$).

The Kozeny–Carman equation has a limited range of applications owing to its strict application only to loose sand. Estimating the specific surface area of the grain in consolidated rock formations is complicated, and, most importantly, it cannot be directly measured by logging. Timur (1968) created a modified version of the original equation based on typical borehole logs as a result:

$$k_{\text{Timur}} = a^b\left(\frac{1}{S_{\text{Wirr}}}\right)^c, \tag{2}$$

where k_{Timur} is the permeability (mD); $a = 10^4$ is a formation-dependent correction coefficient dependent on Archie's (1942) coefficients m and n (mD ms^2); b = 4.4 and c = 2.0 are regression coefficients statistically evaluated from laboratory experiments; ϕ (%) is the porosity obtained from NPHI, RHOB, or DT logs, and S_{Wirr} (%) is the irreducible water saturation, which can be estimated from the NMR log or using the water saturation (S_{W}) vs. porosity (ϕ) cross plot (Buckles, 1965). The equation applies solely over zones with S_{Wirr}, i.e., hydrocarbon zones on top of the transition zone (Kennedy, 2015).

Posteriorly, Coates et al. (1999), following Timur's model, developed a model for permeability based on the NMR log through the following equation:

$$k_{\text{TimurCoates}} = a^b\left(\frac{\text{FFI}}{\text{BVI}}\right)^c, \tag{3}$$

where a, b, and c have the same values as those shown in Timur's equation. The free fluid index (FFI) is the producible part of porosity or the productive potential volume in the saturated rock for a given capillary pressure (%). The bound volume irreducible (BVI) is the nonproducible part of porosity or the volume of the fluids trapped inside the porous structure by capillary forces (%). Both values are determined based on the T2cutoff time, as shown in the yellow and blue shading of Suppl. Mat., Fig. 3. In the equation, they are defined as

$$\text{FFI} =_{\text{NMR}} -\text{BVI} \text{ and} \tag{4}$$

$$\text{BVI} =_{\text{NMR}} S_{\text{Wirr}}, \tag{5}$$

where ϕ_{NMR} is the porosity (%) measured through the NMR log.

The study scheme started linearizing permeability equations 2 and 3 using an operator called "the Jacobian matrix" (A), formed by partial derivatives of the linearized equation about the parameters to be calculated, a, b, and c. The workflow designed for this work is shown in Suppl. Mat., Fig. 3. Following it, the dataset used in this study includes geophysical well logs, such as caliper (CAL), gamma-ray (GR), neutron porosity (NPHI), density (RHOB), sonic (DT), photoelectric (PEF), shallow resistivity (RXO), deep resistivity (RT), and NMR T2 distribution. Experimental porosity (ϕ_{LAB}) and permeability (k_{LAB}) data were also used, measured in the laboratory from core samples with helium gas expansion. These measurements were used to assess the quality of the simulations. Thus, the first stage of the work was reservoir characterization based on the analysis of the logs with the use of the Interactive Petrophysics – IP (Geoactive…, 2021) software. This preliminary interpretation exposed important reservoir characteristics, such as top, bottom, carbonate mud presence, water saturation, porosity, and presence of oil.

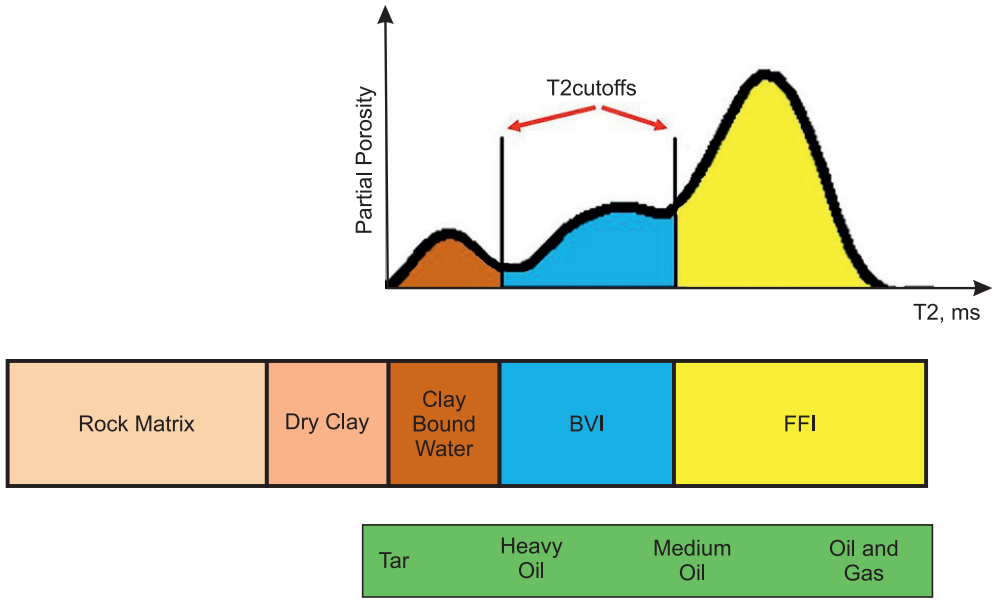

Fig. 2. Free fluid index (FFI, yellow shaded) and bound volume index (BVI, blue shaded) zones in the nuclear magnetic resonance (NMR) porosity distribution based on the T2cutoff time.

Next, several porosity estimates were made based on NPHI, RHOB, DT, and NMR logs, aiming to find the best correlation ϕ_{LAB} and choose it for use in the Timur and Timur–Coates permeability estimation (Kennedy, 2015). An NMR log was also used to estimate the FFI and BVI, essential parameters for estimating permeability through the Timur–Coates model (Fig. 2). The reservoir was then divided into flow zones (FZ), each having its own cutoff time (T2cutoff), which is used to determine more realistic values for the BVI and FFI (Carrasquilla et al., 2012).

In the case of borehole logging, the inverse problem refers to the determination of the physical properties of the geologic medium crossed by a borehole, given the data of response of this environment to the logging tools (Oliver et al., 2008). This problem is considered underdetermined, because there are more model variables than the amount of information obtained through an inversion process. The solution is nonunique, since the optimization approach has many solutions for every log when they are linearly independent. The problem is also ill-posed, because it is impossible to fit the associated data (Lavrentiev, 1967). The ridge regression scheme was used to carry out the deterministic inversion, a linear model the estimator of which has biased coefficients with lower variance than the conventional least squares. It includes positive weights along the diagonal of the covariance matrix, unlike the standard least squares estimator (Suppl. Mat., Fig. 4). The ridge regression approach is an instance of Tikhonov's (1963) regularization, with the addition of conversion into a correlation matrix, which is optional but allows comparisons of the magnitude of the smoothing coefficient between models. In this scenario, the ridge estimator is given by Tarantola (2004):

$$x = \left(A^{\mathrm{T}} A + I\right)^{-1} A^{\mathrm{T}} y + , \tag{6}$$

where x is the parameter vector of dimension p; y is the observation vector of dimension p; A is the Jacobian matrix of dimension $p \times q$; λ is the regularization parameter; T means transposed; ε is the error or residuals; and I is the identity matrix. The inversion code was developed in the Matlab (2016) platform, for which it was necessary to input the variables of the initial parameters (a_0, b_0, and c_0), the acceptable margin of error (ε), and the smoothing parameter (λ). The algorithm output was the estimated permeability curve, with the parameters a, b, and c being evaluated when the inversion stabilizes or converges. There are other methods for solving the corresponding systems of linear equations, for example, the singular value decomposition, which makes it possible to obtain a solution with a minimum norm. In contrast, in the case of the Tikhonov regularization, the resulting solution will depend on parameter λ, the value of which is rather difficult to determine (Tavakoli and Reynolds, 2011).

The stochastic inversion used the FL approach, and the uncertainty analysis was made with MC. Fuzzy logic is used to develop a forward model, based on the basic logs, to estimate the permeability of the reservoir, and measurements of the core samples are made to assess the quality of the adjustments. Fuzzy logic is an ex-

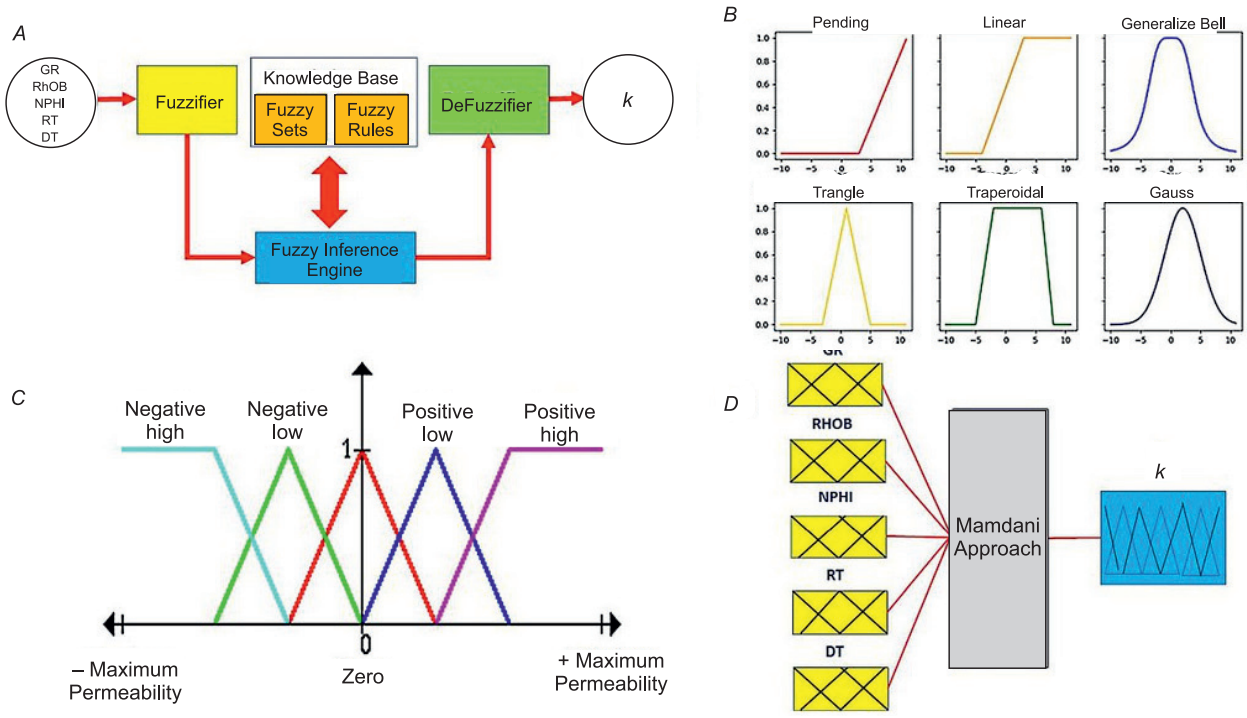

Fig. 3. Fuzzy logic approach:

A – General scheme with conventional logs as input and permeability as output; *B* – types of membership functions (adapted from https://github.com/VManuelSM/Membership-functions); *C* – rules (adapted from https://www.geocities.ws/hemakumar_b37/fuzzy); *D* – Mamdani controller.

tension of conventional Boolean logic developed as a means of modeling uncertainty through the concept of "partial truth," that is, truth values between "completely true" and "completely false" (Zadeh, 1965). This concept makes it possible to consider extreme values and infinite possibilities between the true and the false. The models or sets are mathematical means of representing vagueness and imprecise information, hence the term "fuzzy," which can recognize, represent, manipulate, interpret, and use data and information that are vague and lack certainty (Padilla et al., 2022). In fuzzy techniques, each term is described by a function that assigns to each possible value x of the corresponding quantity a degree $\mu(x)$ from the interval [0, 1], to which this value satisfies the related property. Here, (a) 1 means that the property is satisfied; (b) 0 means that the property is not satisfied; and (c) values between 0 and 1 correspond to intermediate degrees of confidence. The corresponding function $\mu(x)$ is a membership function or fuzzy. The rules usually combine inaccurate statements using logical connectives like "and," "or," "not," "if-then," "implies," etc. The mathematics involved is part of a normal distribution, which is given by Cuddy and Glover (2002):

$$P(x) = \frac{e^{-(x-\bar{x})^2/2\sigma^2}}{\sigma\sqrt{2\pi}}, \tag{7}$$

where $P(x)$ is the probability of an x observation being measured in the dataset described by the arithmetic mean $\bar{x}$ and standard deviation σ. A Gaussian, or normal, distribution curve estimates the relative likelihood, fuzziness, that an observation belongs to a specific dataset. The dataset can be divided into smaller parts called "bins," so that the probability of an observation belonging to a given bin can be calculated from Eq. 6 by replacing the mean and the standard deviation by $\bar{x}_b$ and σ_b. These parameters are derived from the calibrating or conditioning dataset using the conventional statistics by the normal distribution. The most well-known fuzzy system is the Mamdani rule-based one, the inference of which was first introduced as a control system for the method by synthesizing a set of linguistic control rules obtained from experienced human operators. In this system, the output of each rule is a fuzzy set (Fig. 3*A*). The following rules are used: (a) fuzzify all input values into fuzzy membership functions (Fig. 3*B*, *C*), (b) execute all applicable rules in the rule base to compute the fuzzy output functions (Fig. 3*D*), (c) defuzzify the fuzzy output functions to get "crisp" output values (Fig. 3*A*) (Mamdani and Assilian, 1975).

Monte Carlo simulation performs sensitivity analysis through random parameter variation. It is a technique for studying how a model responds to randomly generated inputs. Stochastic inversion techniques are widely used to assess the permeability of complex heterogeneous systems. For example, Tyler et al. (1996), Li et al. (2005), McKenna and Reeves (2006), and Bruckmann and Clauser (2020) worked on this theme. This approach is used for dealing with the variability and complexity of the parameters that control permeability, such as porosity, pore throats, and system connectivity. This estimate section will develop the stochastic inversion through the FL scheme as the forward problem and the MC uncertainty analysis. In this case, its vagueness evaluation is applied to the FL model to assess the degree of confidence of the evaluated model. It involves a three-step process: (a) randomly generate "N" inputs, sometimes called scenarios (Suppl. Mat., Fig. 5*A*), (b) run a simulation for each of the "N" inputs (Suppl. Mat., Fig. 5*B*), and (c) aggregate and assess the outputs from the simulations (Suppl. Mat., Fig. 5*C*).

It is assumed that the samples are taken from a normalized distribution function f_x, such that the probability of a value of the variable being between x and $x + dx$ is given by $f_x dx$. If the value x is in a range $[a, b]$, then the total probability will be

$$\int_a^b f_x dx = 1, \tag{8}$$

The cumulative distribution function can be defined as

$$F_x = \int_a^x f_x dx, \tag{9}$$

From these settings, you can generate a random number R_f and equal F_x (Kroese et al., 2014). Thus, the representative value for variable x will be obtained from

$$F_x = R_f \,. \tag{10}$$

The distribution to be chosen depends on the analyzed application, the Gaussian being one of the most used (Suppl. Mat., Fig. 5*D*). By generating random variables, it is possible to simulate many probabilistic models through this process (Prügel-Bennett, 2019). The possible scenarios are simulated with this random generator, considering the type of distribution chosen (normal), the variation interval (10%), the input data (logs), and the number of simulations (500).

The goodness of fit for the estimates shows the degree of error and correlation between observed and calculated data. Thus, the statistics metric of the forecast was calculated with the Pearson correlation coefficient (R), root mean square error (RMSE), mean absolute error (MAE), and Willmott's agreement index (d), all checked with ϕ_{LAB} and k_{LAB} laboratory data (Devlin et al., 1975). The coefficient R measures linear correlation or degree of association between two datasets and two variables. Root mean square error is frequently used to measure the differences between values predicted by an estimator and observed values. At the same time, MAE measures errors between paired observations expressing the same phenomenon. Meanwhile, d is a standardized measure of the degree of model prediction error, which varies between 0 and 1, and it represents the ratio of RMSE and the potential error (Willmott, 1984). The main difference between RMSE and MAE is that the first is more sensitive to observations with huge errors. At the same time, MAE is more robust to observations with values very distant from most other observations (outliers).

RESULTS

Reservoir evaluation. Numerous works on geological and petrophysical topics have been published on this oilfield, including those by Mohriak et al. (1990), Gunter et al. (1997), Cainelli and Mohriak (1999), Guardado et al. (2000), Blauth et al. (2011), Bueno et al. (2014), and Carrasquilla and de Abreu (2023). These authors stated that this reservoir can be divided into two main zones (Fig. 4, track 2), designated as zone 1 (red) and zone 2 (green). This figure also displays the CAL, GR, RXO, RT, RHOB, NPHI, DT, and PEF logs on tracks 3 to 6 that were used for this assessment. The GR log in zone 1 has a mode around 85 °API and values ranging from 45 to 180 °API, typical of areas with high mud content, which are, therefore, radioactive. Zone 2 has, meanwhile, a mode around 25 °API and values ranging from 17 to 55 °API, which are low radioactivity levels appropriate for the carbonate reservoir (track 3). At the same time, the RXO and RT logs show two types of behavior (track 4): (a) portions in which RT (red curve) is more significant than RXO (black curve), indicating the contact between the water-based mud fluid and the reservoir hydrocarbons; (b) parts in which these two

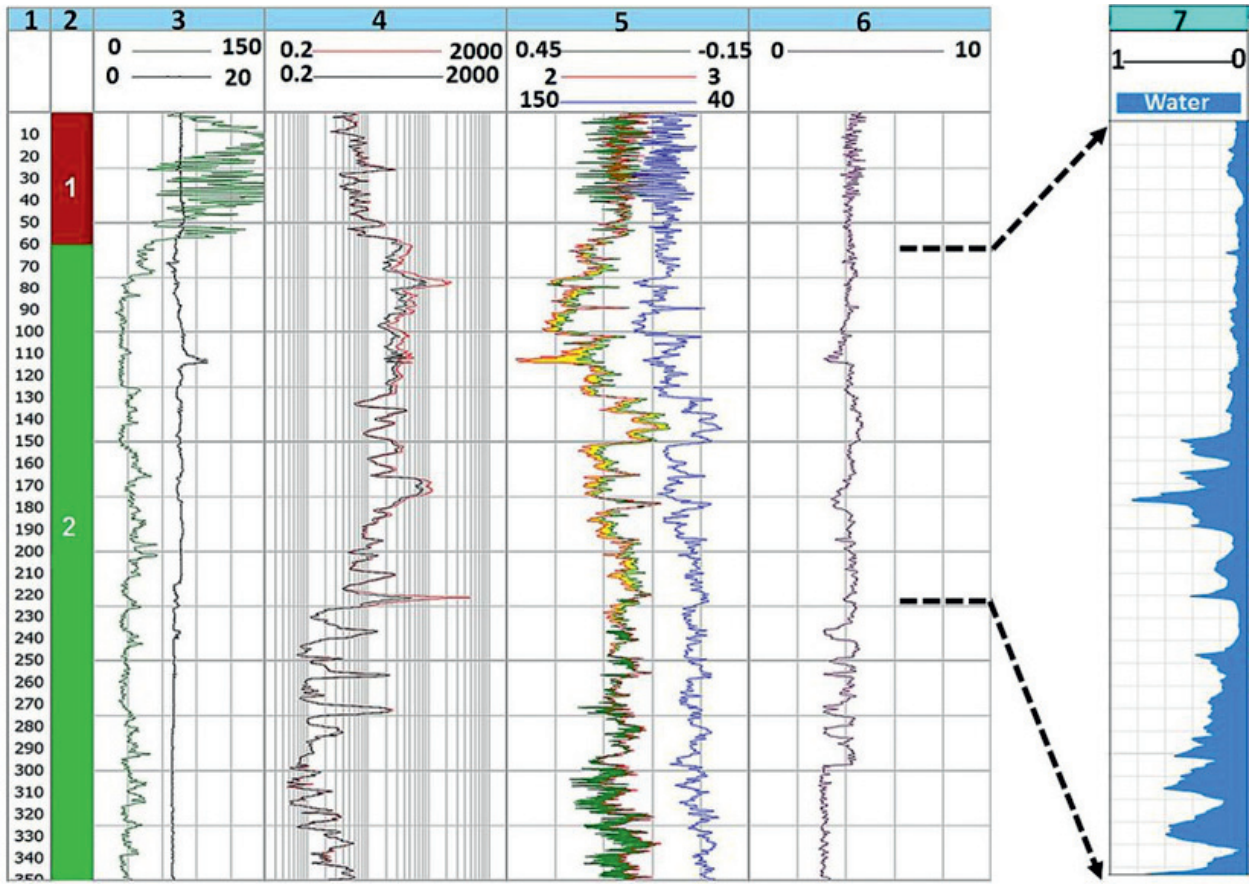

Fig. 4. Well logs were used in the study. Tracks:

1 – depth (m); *2* – zones 1 and 2; *3* – GR (°API, green curve) and CAL (*in*, black curve) logs; *4* – RXO-Shallow (Ohm·m, black curve) and RT-deep resistivity (Ohm·m, red curve) logs; *5* – NPHI (p.u., green curve), RHOB (g/cm^3, red curve), and DT (ms/ft., blue curve) logs; *6* – PEF (B/e, gray curve) log; *7* – Archie S_W (%, blue shaded).

logs overlap, indicating that resistivity near the borehole wall is like that of the formation; i.e., the water-based mud fluid (black curve) gets in touch with the reservoir water (red curve). Crossings between RHOB and NPHI logs along the borehole are shown in track 5, indicating the presence of hydrocarbons (yellow shading) and water (green shading). The DT log also in this track shows many variations throughout the well, which indicates the lithologic alterations. The PEF log is shown in track 6, and their values for limestone, dolomite, and quartz minerals are 5.1, 3.1, and 1.8 1 B/e, respectively (Schlumberger, 2013). The S_W calculation was performed using the Archie (1942) equation, with coefficient values of $a = 1$; $m = 2$; $n = 2.5$; and $R_W = 0.03$ (track 7). Following this track, S_W is < 20% between 60 to 125 m depth (oil zone), gradually increasing until reaching 80% at 145 m depth (aquifer zone). After this analysis, the reservoir section with the most significant potential for hydrocarbon production is identified in zone 2, between 72 and 125 m depth (track 7).

Afterward, two cross plots were made to support the porosity and lithology estimates based on NPHI, RHOB, and DT logs, shown in Fig. 4 (track 5). Figure 6A (Suppl. Mat.) shows cross plot NPHI versus RHOB, with most points falling on the limestone line (LS), others on the dolomite line (DOL), and a few on the sandstone line (SS). The largest cluster indicates that the primary reservoir has porosity indicated on the line between 20 and 25%. This cross plot shows three sections within zone 2: 2a, which presents PEF values close to 5.1 B/e, being predominantly composed of limestone matrix (dark blue rectangle); 2b, considered a transitional zone with alternating PEF values between 5.1 and 3.1 B/e, which shows an overlap of dolomite and limestone matrices (pink triangle), and 2c, with PEF values around 3.1 B/e, formed mainly by dolomites (light blue rectangle). Figure 6 (Suppl. Mat.) shows cross plot NPHI versus DT, with most points falling on the limestone line (LS, dark blue rectangle), others on the dolomite line (DOL, light blue rectangle), and the rest on the sandstone line (SS). The center of the principal cluster in the LS line is also located between 20 and 25% porosity.

Porosity estimates were based on NPHI, RHOB, DT, and NMR logs to find the best fit with ϕ_{LAB} (Suppl. Mat., Fig. 7). Porosity is vital in permeability evaluation, so numerous efforts have been made to derive a gen-

eral relationship between porosity and permeability. Neutron porosity (ϕ_{NPHI}) is shown in track 3 (green line); it is read directly from the log. The density porosity (ϕ_{RHOB}) was estimated using the limestone matrix density (ρ_{ma} = 2.71 g/cm³) and the density of fluid (ρ_{fluid} = 1.19 g/cm³), which is the mud filtrate in the invaded zone (track 4, red line). The sonic porosity (ϕ_{DT}) was estimated using Δt_{ma} = 50 μs/ft. for limestone and Δt_{fluid} = 200 μs/ft. for mud filtrate (track 5, blue line). Track 6 (pink line) shows the total porosity, which was determined through the equation $\phi_{ND} = (\phi_{NPHI} + \phi_{RHOB})/2$ (Schlumberger, 2013). The NMR porosity (ϕ_{NMR}) is given by the area below the relaxation time curve (T2); for this reason, it is essential to precisely determine the T2cutoff time, being 111 ms in this case (track 7, green line). The porosity estimates and their respective goodness of fit statistics about the porosity of core samples are listed in Table 1 (Suppl. Mat.). The best correspondence between the estimated porosities and ϕ_{LAB} is followed by $\phi_{NMR,}$ with R = 0.57; RMSE = 0.03; MAE = 0.02; and d = 0.85. The worst estimate is for ϕ_{DT}, with R = 0.42; RMSE = 0.04; MAE = 0.03; and d = 0.78, which may be due to its lack of ability to detect the presence of vugs or fractures, commonly found in carbonate rocks, the size of which is probably not enough to attenuate the sonic signal (Tiab and Donaldson, 2015). As expected, ϕ_{ND} fit slightly better ϕ_{LAB} than ϕ_{NPHI} and ϕ_{RHOB} individually, perhaps, by the presence of secondary porosity, where moderate values are usually caused by vugs and few fractures (Doveton, 2014). Carrasquilla and Lima (2020) confirmed this pattern by analyzing acoustic image logs, concluding that this oilfield presents heterogeneous zones owing to the high occurrence of vugs at these depths.

Using ϕ_{LAB}, $k_{LAB,}$ and geological information, Nocchi (2012) utilized the Winland (1972) equation to classify the different rock types according to the pore throat radius (r) and to determine the flow zones (FZ). The T2cutoffs were also determined from the NMR log for each FZ using an inverse process (Table 2). These parameters are important, because it is through them that the FFI and BVI are determined, which are required in the Timur–Coates permeability evaluation. Thus, the reservoir was separated into nine FZ used as a basis for finding the BVI and FFI in Suppl. Mat., Table 2 and Fig. 8 (track 2). Track 4 shows the S_{Wirr} evaluation from the NMR log used in the Timur permeability estimate, while track 5 displays the FFI (yellow shaded) and BVI (brown shaded), where free fluid is more abundant than the trapped liquid. The laboratory data for ϕ_{LAB} and k_{LAB} from core samples are shown in tracks 6 and 7 (black dots). The blue curve of track 6 (k_{INT}) interpolates k_{LAB}, which is used in the deterministic inversion with the Timur and Timur–Coates equations. This interpolation is required to solve the system of equations, because k_{LAB} is very spaced, and an almost continuous array is necessary as a function of depth. The red curve in track 7 is ϕ_{NMR}, while the cutoffs of the T2 distribution are shown in track 8, T2cutoff (constant T2, red curve) and T2cutoffgm (T2 geometric mean, light blue curve). T2cutoff was made by the interpreter much faster and more useful in a preliminary interpretation than T2cutoffgm, used in the Schlumberger permeability formula (k_{SDR})

$$k_{SDR} = a\phi_{NMR}^{b}\left(T_{T2cutoffgm}^{c}\right), \tag{11}$$

where a, b, and c are constants with the same meaning as those explained in the previous equations.

Deterministic inversion of permeability. The essential idea of deterministic inversion is to stabilize or converge the parameters b and c of the Timur and Timur–Coates equations from the input or initial parameters b_0 and c_0 in the permeability estimation. In the inverse processes, the initial parameter a_0 remains constant with a value of 1.0×10^4, because it is a scalar constant that has to do with transforming the theoretical Kozeny–Carman equation into the well-log practical cases. A code was developed in the Matlab (2016) platform based on the methodology proposed by de Oliveira (2019) for the S_W estimation and modified for the case of permeability by Guerra (2020). The input parameters shown above were chosen based on the shared values of two equations in the literature. In the case of ε, though there was no information about the acquisition error, it was considered low and chosen with a value of 10%. The regularization parameter λ is a positive quantity less than one (usually less than 0.3), and it varies during the execution of the inverse process. The algorithm was developed as output to display the stabilized parameters b and c, the convergent estimate, and the fit statistic parameters (R, RMSE, MAE, and d).

Two simulations with the Timur equation were performed, the first with the entire reservoir interval and the second using the division of the reservoir into FZ. The other simulation was made with the traditional model of Timur and Coates. The simulated permeability curves with this inversion procedure are shown in Fig. 9 (Suppl. Mat.) for the Timur original equation (track 4, green curve), for the Timur–Coates equation (track 5, red curve), and the Timur equation dividing the reservoir into FZ (track 6, blue curve). The three simulations plotted with k_{LAB} (black dots) are shown in the respective tracks, and all the estimates are in track 7. Table 3 (Suppl. Mat.) shows the input parameters a_0, b_0, and c_0 for each simulation, besides the change of l (regularization parameter) and *in* (number of iterations) for the models of Timur, Timur–Coates, and Timur with flow zones**.** For the Timur model, three simulations were carried out with $a_0 = 1.0 \times 10^4$; b_0 = 5.0; c_0 = 2.0; and *in* = 2, the only parameters that change being l = 500.0, 1.0×10^3, and 1.5×10^3. For the Timur–Coates model,

three simulations were also carried out with $a_0 = 1.0 \times 10^4$; $b_0 = 4.0$; $c_0 = 2.0$; and $in = 5$, with only changes in $l = 1.750 \times 10^3$, 2.375×10^3, and 2.750×10^3. In both cases, iterations were stopped when convergence was reached. For the Timur model with flow zones, owing to experience with previous simulations, three of them were carried out, with $a_0 = 1.00 \times 10^4$; $20.65 < b_0 < -10.22$; and $12.63 < c_0 < -7.26$, the latter two varying in each flow zone. For this model, l and *in* have variations according to each flow zone, $25.00 < l < 0.50$, and $250 < in < 2$.

The statistical results of the goodness of fit are shown in Suppl. Mat., Table 4. This table shows that Timur's estimate with flow zones presents the best results with $R = 0.55$; RMSE = 210.88; MAE = 116.66; and $d = 0.84$, with FZ1, FZ7, and FZ9 being the best-defined and FZ2, FZ5, and FZ8 the worst. Next comes Timur's evaluation for the entire reservoir ($R = 0.40$; RMSE = 401.57; MAE = 164.68; $d = 0.56$) and, finally, the Timur–Coates model ($R = 0.39$; RMSE = 424.30; MAE = 123.57; $d = 0.52$). Thus, these results show that deterministic inversion is a tortuous process for permeabilities, but dividing reservoirs into flow zones is a good strategy for improving permeability estimation.

Stochastic inversion of permeability. At the start, to make the stochastic inversion of permeability, it was necessary to develop the FL forward model based on the input logs shown above and k_{LAB} to check the quality of the fit. The choice of bins is given according to the data of the higher reliability present model, i.e., the core samples. According to Cuddy and Glover (2002), the number of bins will depend on the number of core samples available, and a reasonable number of samples per bin is about 30. Since the present study has data from 99 core samples, three bins would be sufficient to generate a consistent model. The results for simulation 1 of the probabilistic model are in Suppl. Mat., Fig. 10 (tracks 3 and 4), plotted along with k_{LAB} (black dots). In track 3, $k_{FL\_S1\_ml}$ (green curve) is the most likely result, and $k_{FL\_S1\_av}$ (red curve) represents the average between the curves of the highest $k_{FL\_S1\_mlH}$ and lowest $k_{FL\_S1\_mlL}$ probability of $k_{FL\_S1\_ml}$, which is considered a reference for the model. In track 4, $k_{FL\_S1\_ml}$ (green curve), $k_{FL\_S1\_mlH}$ (gray curve), and $k_{FL\_S1\_mlL}$ (gray curve) are plotted, which are essential for the evaluation, because it is by the use of them that the variation, or inaccuracy, is shown through the yellow shaded region or fuzziness. It is seen in this figure that the simulation generated better permeability estimates at various intervals along the wellbore. This feature is more evident in FZ1 and FZ9 at the beginning and end of the studied borehole range, where $k_{FL\_S1\_ml}$ and $k_{FL\_S1\_av}$ curves do not show variation and remain the same. The statistics of the goodness of fit of this simulation is $R = 0.35$; RMSE = 320.27; MAE = 190.93; and $d = 0.73$, which is a bad estimate (Suppl. Mat., Table 5).

A second simulation was performed with six bins and the same input logs. The improvement was significant, as observed in tracks 5 and 6 of Fig. 10 (Suppl. Mat.). The zones in simulation one ($k_{FL\_S1\_ml}$, three bins) were not well adjusted, but simulation two ($k_{FL\_S2\_ml}$, six bins) has a more excellent approximation with k_{LAB}. Track 5 shows $k_{FL\_S2\_ml}$ (green curve) and $k_{FL\_S2\_av}$ (red curve), plotted along with k_{LAB} (black dots). As mentioned in simulation 1, in simulation 2, the $k_{FL\_S2\_av}$ curve represents the average between $k_{FL\_S2\_mlH}$ and $k_{FL\_S2\_mlL}$, and $k_{FL\_S2\_ml}$ is the most likely result. The statistics of the goodness of fit of this simulation is $R = 0.87$; RMSE = 156.81; MAE = 74.60; and $d = 0.92$, which is a reasonable estimate and much better than $k_{FL\_S1\_ml}$ with $R = 0.35$; RMSE = 320.27; MAE = 190.23; and $d = 0.73$ (Table 5). Track 6 displays $k_{FL\_S2\_ml}$ (green curve), $k_{FL\_S2\_mlH}$ (gray curve), $k_{FL\_S2\_mlL}$ (gray curve), and the estimated imprecision through the yellow shaded region (fuzziness).

In an exploratory analysis, it is impossible to be entirely sure of a decision, but reasonable estimates can be made. For this reason, probabilistic estimates are often used in decision-making. The MC uncertainty analysis assumes this role by simulating potential scenarios and evaluating their degree of probability. Thus, this stage of the work aims to assess the FL model developed through the analysis of uncertainties by MC. Possible scenarios are simulated through a random generator based on the type of distribution chosen, the margin of variation, input data, and the number of simulations. The distribution chosen was Gaussian (normal), because the generated values are expected to represent the real data, presenting smoother ends and higher density in intermediate values. The margin of variation of the scenarios was 50 lower and 50 higher at the reference values, i.e., the confidence interval in track 5 of Fig. 11 (Suppl. Mat.). The input data were the curves generated in the FL model, the logs used in the previous analyses, and the permeability values of core samples. As explained, the MC method stabilizes in a certain number of iterations, when it begins to generate exceedingly minor variations. In this study, the total number of iterations used was 500, since for larger values the differences were insignificant.

The simulation results can be found in Fig. 11 (Suppl. Mat.) (tracks 4 and 5). In track 4, the $k_{FL\_S2\_av\_P10}$, $k_{FL\_S2\_av\_P50}$, and $k_{FL\_S2\_av\_P90}$ curves represent the 10, 50, and 90 percentiles of the lowest values of all 500 simulations, respectively. In track 5, the confidence interval of the simulations is observed, where $k_{FL\_S2\_av\_me}$ and $k_{FL\_S2\_av\_pe}$ represent the negative and positive variations about the $k_{FL\_S2\_av}$, respectively. The P10, P50, and P90 curves are fundamental in understanding how the values are distributed in the sample (track 4). It is necessary to note that the program classifies all the results for each depth level and then calculates the value of each

of the three percentiles to evaluate these parameters. A widespread error in this type of analysis is to confuse the percentiles with a probability of occurrence. The P90 does not mean that the estimate has a 90% chance of occurring, but rather that the $k_{FL\_S2\_av\_P90}$ curve at that depth represents this percentile of the values calculated in the distribution curve. Once the distribution is normal, that is, a symmetric distribution, the best parameter to evaluate this dataset is P50 ($k_{FL\_S2\_av\_P50}$). Thus, looking at $k_{FL\_S2\_av\_P50}$ (red) and $k_{FL\_S2\_av}$ (black dashed, track 4), we notice that the curves show similar behavior in much of the studied interval. The most significant differences between the estimate and the real data are shown, too. In a brief comparison, in Table 3 (Suppl. Mat.) of the deterministic inversion by FZ, the algorithm could not stabilize the coefficients in these zones. Still, in the stochastic inversion, it was possible to perform a better estimate of permeability, even if presenting low reliability.

CONCLUSIONS

Deterministic and stochastic inversions were employed to estimate the permeability of a carbonate reservoir in this work. A preliminary reservoir analysis was conducted on well-log data to determine the mudstone concentration, water saturation, porosity, and hydrocarbon presence of the reservoir. The NMR porosity was the most effective method for estimating the permeability, according to an analysis of the fit error between the estimated and the core sample porosities. Based on the ridge regression scheme, the Timur and Timur–Coates permeability equation coefficients were calculated as part of the deterministic inversion process. Both algorithms failed to replicate the permeability behavior at the reservoir edges and some intervals inside the reservoir when the reservoir was viewed as a single unit. The permeability values differed slightly in each flow zone when the reservoir was sectioned. The Timur equation exhibits a better correlation with the core data (R = 0.41; RMSE = 333.48; MAE = 95.56; and d = 0.55) when compared with the Timur–Coates model (R = 0.39; RMSE = 355.28; MAE = 79.35; and d = 0.51). Timur's flow zone model outperformed the other two (R = 0.55; RMSE = 210.88; MAE = 116.66; and d = 0.84), but this method failed to bring the coefficients into convergence in some flow zones. Deterministic inversion has a reduced capacity to adjust to significant variations in the permeability values along the borehole. As a result, a stochastic inversion was constructed using the forward problem with the fuzzy logic scheme and the uncertainty analysis of Monte Carlo. The processes started developing the fuzzy model based on the log data as input and the permeability measured in samples to support the results. The study has demonstrated that the fuzzy model with three bins shows worse results than deterministic inversion, with R = 0.35; RMSE = 320.27; MAE = 190.93; and d = 0.73. Despite that, the guess with six bins consistently estimated the permeability in flow zones with R = 0.87; RMSE = 156.81; MAE = 74.60; and d = 0.92, which the deterministic inversion could not do. The Monte Carlo uncertainty analysis was then used to evaluate this model, which had the best correlation with the real data. The goodness of fit analysis has shown that the stochastic process succeeds in the flow zones where the deterministic inversion is unsuccessful. It has demonstrated that the estimate is located between 50% and 90% probability of occurring, usually closer to 90%. Finally, it is possible to see that the deterministic inversion cannot match the critical permeability alterations when analyzed to the stochastic inversion. The random approach can perform an accurate permeability assessment, because it is a robust solution with reliable parameters, which validate the estimation stability.

The authors thank the Brazilian National Research Agency (CNPq) for the research grant, the Petroleum Engineering and Exploration Laboratory (UENF–LENEP) for the computing infrastructure, the Geophysical Science and Technology Institute (INCT-GP) for the support, and Geoactive Limited for the academic license of Interactive Petrophysics (IP) software.

REFERENCES

Adams, S.J., 2005. Quantifying petrophysical uncertainties. SPE Asia Pacific Oil Gas Conf. Exhibition, Jakarta, Indonesia, Pap. SPE-93125-MS, doi: 10.2118/93125-MS.

Ahangar-Asr, A., Faramarzi, A., Mottaghifard, N., Javadi, A., 2011. Modeling of permeability and compaction characteristics of soils using evolutionary polynomial regression. Comput. Geosci. 37, 1860–1869, doi: 10.1016/j.cageo.2011.04.015.

Alkinani, H., Al-Hameedi, A.T., Dunn-Norman, S., Aldin, M., Gokaraju, D., Guedez, A., Alattar, A., 2022. Regularized ridge regression models to estimate static elastic moduli from wireline measurements: case study from Southern Iraq. J. Pet. Explor. Prod. Technol. 12, 1759–1773, doi: 10.1007/s13202-021-01434-5.

Amaefule, J., Altunbay, M., Tiab, D., Kersey, D., Keelan, D., 1993. Enhanced reservoir description: using core and log data to identify hydraulic (flow) units and predict permeability in uncored intervals/wells. SPE Annu. Tech. Conf. Exhibition, Houston, Pap. SPE 26436, pp. 205–220, doi: 10.2118/26436-MS.

Archie, G., 1942. The electrical resistivity log as an aid in determining some reservoir characteristics. J. Pet. Technol. 146, 54–62, doi: 10.2118/942054-G.

Bernabé, Y., Li, M., Maineult, A., 2010. Permeability and pore connectivity: A new model based on network simulations. J. Geophys. Res. 115, B10203, doi: 10.1029/2010JB007444.

Blauth, M., Faria, R., Maul, A., Monteiro, M., Pittella, M., Carneiro, S., Tibana, P., 2011. Workflow for geological characterization and modeling of the Albian carbonate reservoirs from offshore Campos Basin, Brazil. AAPG Int. Conf. Exhibition, Milan, Italy, AAPG Search and Discovery, Article 90135.

Bruckmann, J., Clauser, C., 2020. Ensemble-based stochastic permeability and flow simulation of a sparsely sampled hard-rock aquifer supported by high performance computing. Hydrogeol. J. 28, 1853–1869, doi: 10.1007/s10040-020-02163-5.

Bruhn, C., Gomes, J., Lucchese, C., Jr., Johann, P., 2003. Campos Basin: Reservoir characterization and management-historical overview and future challenges. Offshore Technol. Conf., Houston, TX. Pap. OTC-15220-MS, 1–14, doi: 10.4043/15220-MS.

Buckles, R., 1965. Correlating and averaging connate water saturation data. J. Can. Pet. Technol. 4, 42–52, doi: 10.2118/65-01-07.

Bueno, J., Honório, B., Kuroda, M., Vidal, A., Leite, E., 2014. Structural and stratigraphic feature delineation and facies distribution using seismic attributes and well log analysis applied to a Brazilian carbonate field. Interpretation 2, 1–10, doi: 10.1190/INT-2013-0087.1.

Cainelli, C., Mohriak, W., 1999. Some remarks on the evolution of sedimentary basins along the Eastern Brazilian continental margin. Episodes 22, 206–216, doi: 10.18814/epiiugs/1999/v22i3/008.

Cao, Z., Kruczek, B., Thibault, J., 2022. Monte Carlo simulations for the estimation of the effective permeability of mixed-matrix membranes. Membranes 12, 1053, doi: 10.3390/membranes12111053.

Carman, P., 1937. Fluid flow through granular beds. Trans. Inst. Chem. Eng. 15, 150–166, doi: 10.1016/S0263-8762(97)80003-2.

Carrasquilla, A., Lima, R., 2020. Basic and specialized geophysical well logs to characterize an offshore carbonate reservoir in the Campos Basin, southeast Brazil. J. South Am. Earth Sci. 98, 102436, doi: 10.1016/j.jsames.2019.102436.

Carrasquilla, A., de Abreu, C., 2023. Estimation of the size and type of porosity in an Albian carbonate reservoir of the Campos Basin, Southeastern Brazil. Russ. Geol. Geophys. 64 (1), 123–132, doi: 10.2113/RGG20214382.

Carrasquilla, A., Nocchi, G., Briones, V., Torres, M., Franco Filho, N., Schuab, F., Sanchez, P., 2012. Petrophysical studies in the characterization of carbonate reservoirs of Campos Basin – Brazil. AAPG/SPE/SEG Hedberg Res. Conf. Fundamental Controls on Flow in Carbonates, Provence, France, Search and Discovery, Article 120034.

Coates, G., Denoo, S., 1981. The producibility answer product. The Tech. Rev. 29 (2), 54–63.

Coates, G., Dumanoir, J., 1974. A new approach to improved log-derived permeability. The Log Analyst 15, 17–31.

Coates, G., Xiao, L., Prammer, M., 1999. NMR Logging: Principles and Applications. Halliburton Energy Services, Houston.

Cuddy, S., Glover, P., 2002. The application of fuzzy logic and genetic algorithms to reservoir characterization and modeling, in: Wong, P., Aminzadeh, F., Nikravesh, M. (Eds.), Soft Computing for Reservoir Characterization and Modeling. Studies in Fuzziness and Soft Computing, Vol. 80. Physica, Heidelberg, pp. 219–241, doi: 10.1007/978-3-7908-1807-9_10.

Devlin, S., Gnanadesikan, R., Kettenring, J., 1975. Robust estimation and outlier detection with correlation coefficients. Biometrika 62, 531–545, doi: 10.1093/biomet/62.3.531.

de Oliveira, R., 2019. Determination of Archie Equation Parameters for Clean and Clayey Reservoirs. Graduation Thesis, UENF/LENEP, Macaé–RJ, Brazil [in Portuguese].

Dias, J., Scarton, J., Esteves, F., Carminatti, M., Guardado, L., 1990. Aspects of tectonic-sedimentary evolution and hydrocarbon development in the Campos Basin, in: Gabaglia, G., Milani, E. (Eds.), Origin and Evolution of Sedimentary Basins. Petrobras, CenSuD, Rio de Janeiro, pp. 333–360 [in Portuguese].

Doveton, J., 2014. Principles of Mathematical Petrophysics. International Association for Mathematical Geosciences, Studies in Mathematical Geosciences, Oxford Univ. Press, doi: 10.1093/oso/9780199978045.001.0001.

Esmailzadeh, A., Ahmadi, S., Rooki, R., Mikaeil, R., 2017. Oil reservoir permeability estimation from well logging data using statistical methods (a case study: South Pars oil reservoir). Civ. Eng. J. 3, 831–840, doi: 10.28991/cej-030918.

Fazelabdolabadi, B., Bagherzadeh, H., Shahrabadi, A., Samimi, S., 2019. On the prediction of pseudo relative permeability curves: meta-heuristics versus Quasi-Monte Carlo. Oil Gas Sci. Technol. Rev. IFP Energies Nouvelles 74, 42, doi: 10.2516/ogst/2019014.

Francioli, A., Carrasco, A., 2019. Uncertainty quantification of petrophysical parameters obtained from well logging and core data from carbonate formation using Monte Carlo simulation and fuzzy logic, in: Proceedings of the 16th International Congress of the Brazilian Geophysical Society. SBGf, Rio de Janeiro.

Geoactive Limited, Interactive Petrophysics version 4.0, User's Manual, 2021.

Glover, P., Walker, E., 2009. Grain-size to effective pore-size transformation derived from electrokinetic theory. Geophysics 74, E17–E29, doi: 10.1190/1.3033217.

Guardado, L., Gamboa, L., Lucchesi, C., 1989. Petroleum geology of the Campos Basin, a model for a producing Atlantic-type basin, in: Edwards, J.D., Santogrossi, P.A. (Eds.), Divergent/Passive Margin Basins. AAPG, Tulsa, pp. 3–80, doi: 10.1306/M48508C1.

Guardado, L., Spadini, A., Brandão, J., Mello, M., 2000. Petroleum system of the Campos Basin, Brazil, in: Mello, M.R., Katz, B.J. (Eds.), Petroleum Systems of South Atlantic Margins. AAPG Mem. 73, 317–324, doi: 10.1306/M73705C22.

Guerra, R., 2020. Deterministic and Stochastic Inversion in the Evaluation of Permeability in a Carbonate Reservoir. Master's Thesis, UENF/LENEP, Macaé–RJ, Brazil [in Portuguese].

Gunter, G., Finneran, J., Hartmann, D., Miller, J., 1997. Early determination of reservoir flow units using an integrated petrophysical method. SPE Annu. Tech. Conf. Exhibition, SPE-38679-MS, San Antonio, TX, pp. 1–8, doi: 10.2118/38679-MS.

Hambalek, N., Gonzalez, R., 2003. Fuzzy logic applied to lithofacies and permeability forecasting case study: sandstone of Naricual Formation, El Furrial Field, Eastern Venezuela Basin. SPE Lat. Am. Caribb. Pet. Eng. Conf., Port-of-Spain, Trinidad and Tobago, Pap. SPE-81078-MS, doi: 10.2118/81078-MS.

Huang, Z., Shimeld, J., Williamson, M., Katsube, J., 1996. Permeability prediction with artificial neural network modeling in the Venture gas field, offshore eastern Canada. Geophysics 61, 422–436, doi: 10.1190/1.1443970.

Ilkhchi, A.K., Rezaee, M., Moallemi, S., 2006. A fuzzy logic approach for estimation of permeability and rock type from conventional well log data: an example from the Kangan reservoir in the Iran Offshore Gas Field. J. Geophys. Eng. 3, 356–369, doi: 10.1088/1742-2132/3/4/007.

Inyang, U., Cortez-Montalvo, J., Dusterhoft, R., Apostolopoulou, M., Striolo, A., Stamatakis, M., 2019. A kinetic Monte Carlo study to investigate the effective permeability and conductivity of microfractures within unconventional reservoirs. SPE Oklahoma City Oil and Gas Symp. Held in Oklahoma City, OK, Pap. SPE-195220-MS, doi: 10.2118/195220-MS.

Johnson, D., Koplik, J., Schwartz, L., 1986. New pore-size parameter characterizing transport in porous media. Phys. Rev. Lett. 57, 2564–2567, doi: 10.1103/PhysRevLett.57.2564.

Katz, A., Thompson, A., 1986. Quantitative prediction of permeability in porous rock. Phys. Rev. B: Condens. Matter 34, 8179–8181, doi: 10.1103/physrevb.34.8179.

Kennedy, M., 2015. Practical Petrophysics. Developments in Petroleum Science. Elsevier, Amsterdam, Vol. 62.

Kozeny, J., 1927. Über die kapillare Leitung des Wassers im Boden (Aufstieg, Versickerung und Anwendung auf die Bewässerung). Sitzungsber. Akad. Wiss., Math. Naturwiss. Kl., 136 (2a), 271–306.

Kroese, D., Brereton, T., Taimre, T., Botev, Z.I., 2014. Why the Monte Carlo method is so important today. Wiley Interdiscip. Rev. Comput. Stat. 6, 386–392, doi: 10.1002/wics.1314.

Kumar, B., Varghese, J., 2005. Application of Monte Carlo simulation to quantify uncertainties in petrophysical deliverables. Geohorizons, 24–26.

Lacentre, P., Carrica, P., 2003. A method to estimate permeability on uncored wells based on well logs and core data. SPE Latin Am. Caribb. Pet. Eng. Conf., Port-of-Spain, Trinidad and Tobago, April 2003, SPE-81058-MS, doi: 10.2118/81058-MS.

Lavrentiev, M.M, 1967. Some Improperly Posed Problems of Mathematical Physics. Springer, New York, doi: 10.1007/978-3-642-88210-4.

Lee, S., Datta-Gupta, A., 1999. EF characterization and permeability predictions in carbonate reservoirs: role of multivariate analysis and nonparametric regression. SPE Annu. Tech. Conf. Exhibition, Houston, TX, SPE-56658-MS, doi: 10.2118/56658-MS.

Li, Y., LeBoeuf, E., Basu, P., Mahadevan, S., 2005. Stochastic modeling of the permeability of randomly generated porous media. Adv. Water Resour. 28, 835–844, doi: 10.1016/j.advwatres.2005.01.007.

Liu, H., 2017. Principles and Applications of Well Logging. Springer, Berlin, doi: 10.1007/978-3-662-53383-3.

Lucia, F.J., 2007. Carbonate Reservoir Characterization. An Integrated Approach. 2nd ed. Springer, Berlin–Heidelberg, doi: 10.1007/978-3-540-72742-2.

Luthi, S., 2001. Geological Well Logs: Their Use in Reservoir Modeling. Springer, Berlin, doi: 10.1007/978-3-662-04627-2.

Mamdani, E., Assilian, S., 1975. An experiment in linguistic synthesis with a fuzzy logic controller. Int. J. Man Mach. Stud. 7, 1–13, doi: 10.1016/S0020-7373(75)80002-2.

Marek, P., Brozetti, J., Guštar, M., Tikalsky, P., 2003. Probabilistic Assessment of Structures Using Monte Carlo Simulation: Background, Exercises and Software. 2nd ed. Inst. Theor. Appl. Mech., Prague.

Matlab, 2016. Matlab Documentation – MathWorks, www.mathworks.com (consulted in December 2021).

McKenna, S., Reeves, P., 2006. Fractured continuum approach to stochastic permeability modeling, in: Coburn, T., Yarus, J., Chambers, R. (Eds.), Stochastic Modeling and Geostatistics: Principles, Methods, and Case Studies, Vol. 2. AAPG Computer Applications in Geology, 5, Tulsa, OK, pp. 173–186.

Mohriak, W., Mello, M., Dewey, J., Maxwell, J., 1990. Petroleum geology of the Campos Basin, offshore Brazil, in: Brooks, J. (Ed.), Classic Petroleum Provinces. Geol. Soc. Spec. Publ. 50, pp. 119–141, doi: 10.1144/GSL.SP.1990.050.01.0.

Morris, R., Biggs, W., 1967. Using log-derived values of water saturation and porosity. Trans. SPWLA 8th Annu. Logging Symp. Denver, CO, pp. 12–14.

Nocchi, G., 2012. Evaluation of Carbonate Reservoir of Campos Basin Integrating Laboratory Data with Well Logs. Master's Thesis, UENF/LENEP, Macaé – RJ, Brazil.

Okubo, J., Lykawka, R., Warren, L., Favoreto, J., Dias-Brito, D., 2015. Depositional, diagenetic and stratigraphic aspects of Macaé Group carbonates (Albian): example from an oilfield from Campos Basin. Braz. J. Geol. 45, 243–258, doi: 10.1590/23174889201500020005.

Oliver, D., Reynolds, A., Liu, N., 2008. Inverse Theory for Petroleum Reservoir Characterization and History Matching. Cambridge Univ. Press, doi: 10.1017/CBO9780511535642.

Padilla, R., Kosheleva, O., Kreinovich, V., 2022. Shall We Use Logical Approach or More Traditional Mamdani Approach in Fuzzy Control: Pragmatic Analysis. Technical Report UTEP-CS-22-41, Computer Science, Univ. Texas at El Paso, https://scholarworks.utep.edu/cs_techrep/1680.

Prügel-Bennett, A., 2019. The Probability Companion for Engineering and Computer Science. Cambridge Univ. Press.

Schlumberger, 2013. Schlumberger's Log Interpretation Charts. Houston, TX.

Schön, J., 2015. Physical Properties of Rocks. 2nd ed. Elsevier, Houston, TX.

Tao, T., Watson, A., 1984. Accuracy of JBN estimates of relative permeability, Part 1 – Error analysis. SPE J. 24, 209–215, doi: 10.2118/11589-PA.

Tarantola, A., 2004. Inverse Problem Theory and Methods for Model Parameter Estimation. SIAM, Philadelphia, PA, doi: 10.1137/1.9780898717921.

Tavakoli, R., Reynolds, A., 2011. Monte Carlo simulation of permeability fields and reservoir performance predictions with SVD parameterization in RML compared with EnKF. Comput. Geosci. 15, 99–116, doi: 10.1007/s10596-010-9200-8.

Tiab, D., Donaldson, E., 2015. Petrophysics: Theory and Practice of Measuring Reservoir Rock and Fluid Transport Properties. 4th ed. Gulf Prof. Publ., Houston, TX.

Tikhonov, A., 1963. Solution of incorrectly formulated problems and the regularization method. Sov. Math. Dokl. 4 (4), 1035–1038.

Timur, A., 1968. An investigation of permeability, porosity, and residual water saturation relationships for sandstone reservoirs. The Log Analyst 9 (4), 8–17.

Tixier, M., 1949. Evaluation of permeability from electric-log resistivity gradients. Oil Gas J. 8, 75–90.

Tyler, K., Sandsdalen, C., Maeland, L., Aasen, J., Siring, E., Barbieri, M., 1996. Integrated stochastic modeling in reservoir evaluation for project evaluation and risk assessment. SPE Annu. Tech. Conf. Exhibition. Denver, CO, SPE-36706-MS, doi: 10.2118/36706-MS.

Vadapalli, U., Srivastava, R., Vedanti, N., Dimri, V., 2014. Estimation of permeability of a sandstone reservoir by a fractal and Monte Carlo simulation approach: a case study. Nonlinear Processes Geophys. 21, 9–18, doi: 10.5194/npg-21-9-2014.

Wang, J., Yan, W., Wan, Z., Wang, Y., Lv, J., Zhou, A., 2020. Prediction of permeability using random forest and genetic algorithm model. CMES-Comp. Model. Eng. Sci. 125, 1135–1157, doi: 10.32604/cmes.2020.014313.

Wendt, W., Sakurai, S., Nelson, P., 1986. Permeability prediction from well logs using multiple regression, in: Lake, L., Carmil, H., Jr. (Eds.), Reservoir Characterization. Orlando Acad. Press, Orlando, FL, pp. 181–221.

Weston, J., Gammerman, A., Stitson, M., Vapnik, V., Vovk, V., Watkins, C., 1999. Support vector density estimation, in: Schölkopf, B., Burghes, C., Smola, A. (Eds.), Advances in Kernel Methods: Support Vector Learning. MIT Press, pp. 293–305.

Willmott, C., 1984. On the evaluation of model performance in physical geography, in: Gaile, G.L., Willmott, C.J. (Eds.), Spatial Statistics and Models, Part of the Theory and Decision Library Book Ser. Springer, Dordrecht, pp. 443–460, doi: 10.1007/978-94-017-3048-8_23.

Winland, H., 1972. Oil accumulation in response to pore size changes, Wey Burn Field, Saskatchewan, in: Field, W. (Ed.), Amoco Production Research Report, No. F72-G25.

Winter, W., Jahnert, R., França, A., 2007. Campos Basin, in: Milani, E., Rangel, H., Bueno, G., Stica, J., Winter, W., Caixeta, J., Pessoa Neto, O. (Eds.), Stratigraphic Charts [in Portuguese]. Petrobras Geosci. Bull., Vol. 15, Issue 2, pp. 511–529.

Wyllie, M., Rose, W., 1950. Some theoretical considerations related to the quantitative evaluation of the physical characteristics of reservoir rock from electrical log data. Pet. Trans., AIME, 189, 105–118.

Yu, B., Zou, M., Feng, Y., 2005. Permeability of fractal porous media by Monte Carlo simulations. Int. J. Heat Mass Transfer 48, 2787–2794, doi: 10.1016/j.ijheatmasstransfer.2005.02.008.

Zadeh, L., 1965. Fuzzy sets. Inf. Control 8, 338–353, doi: 10.1016/S0019-9958(65)90241-X.